arXiv:1510.09165v2 [astro-ph.EP] 25 Mar 2016

On the rotation of co-orbital bodies in eccentric orbits

A. Leleu* P. Robutel* A.C.M. Correia*†

March 28, 2016

Abstract

We investigate the resonant rotation of co-orbital bodies in eccentric and planar orbits. We develop a simple analytical model to study the impact of the eccentricity and orbital perturbations on the spin dynamics. This model is relevant in the entire domain of horseshoe and tadpole orbit, for moderate eccentricities. We show that there are three different families of spin-orbit resonances, one depending on the eccentricity, one depending on the orbital libration frequency, and another depending on the pericenter's dynamics. We can estimate the width and the location of the different resonant islands in the phase space, predicting which are the more likely to capture the spin of the rotating body. In some regions of the phase space the resonant islands may overlap, giving rise to chaotic rotation.

1 Introduction

In 1772, Lagrange has found an equilibrium configuration where three bodies are located at the vertices of an equilateral triangle where they all move with the same orbital period. Gascheau (1843) has proved the stability of this configuration in the case of circular motion, providing a stability criteria for the masses of the bodies. There are two stable configurations for a quasi-circular co-orbital system: the tadpole orbits, where the two bodies librate around the Lagrangian equilibrium; and the horseshoe orbits, named after the shape the trajectories of the bodies describe in the rotating frame. These configurations are stable if the ratio between the sum of the masses of the co-orbitals and the total mass of the system is below $1/27$ for tadpole orbit (Gascheau, 1843) and $\approx 2 \times 10^{-4}$ for horseshoe orbits (see for example

*IMCCE, Observatoire de Paris - PSL Research University, UPMC Univ. Paris 06, Univ. Lille 1, CNRS, 77 Avenue Denfert-Rochereau, 75014 Paris, France

†Departemento de Fìsica, I3N, Universidade de Aviero, Campus de Santiago, 2810-193 Aveiro - Portugal

E-mail: adrien.leleu@obspm.fr; philippe.robutel@obspm.fr and correia@ua.pt

Leleu et al., 2015). For eccentric co-orbitals, the previous configurations continue to exist, but more configurations are possible: quasi-satellite orbits, in which the two bodies appear to have a retrograde orbit around each other (Namouni, 1999; Mikkola et al., 2006); retrograde co-orbitals, where the co-orbitals orbit in opposite direction (Morais and Namouni, 2013); and anti-Lagrange orbits, which, with the eccentric Lagrangian equilibrium, correspond to the two planar Lyapunov families of orbit emanating from the circular Lagrangian equilibrium (Giuppone et al., 2010; Robutel and Pousse, 2013). The first body on a tadpole orbit was found at the L_4 point of Jupiter (Wolf, 1906) and we presently know more than 6000 bodies of this kind in the solar system, in the frame of the restricted three body problem[1]. Bodies in the horseshoe configuration have been discovered around Saturn, where the co-orbitals have commensurable masses (Dermott and Murray, 1981). Until now, no long-term stable example of the three other co-orbitals configuration have been found.

For close-in bodies, tidal interactions slowly modify the rotation and the orbits (e.g. MacDonald, 1964; Correia, 2009). When the rotation rate and the mean motion have the same magnitude, the dissipative tidal torque may be counterbalanced by the conservative torque due to the axial asymmetry of the inertia ellipsoid. In the two-body problem, for circular orbits, the only possibility for the spin is to end at the synchronous resonance (Goldreich and Peale, 1966; Correia and Laskar, 2009). However, for eccentric orbits, the rotation rate can be locked in a half-integer commensurability with the mean motion, usually called spin-orbit resonance (Colombo, 1965; Goldreich and Peale, 1966; Correia and Laskar, 2009) or have a chaotic rotation, as it is the case for Hyperion (Wisdom et al., 1984a). In the co-orbital circular case, the presence of a co-orbital companion can also give rise to non-synchronous spin-orbit resonances due to the orbital libration around the Lagrangian point (see Correia and Robutel (2013)). In this paper we develop an analytic model for the planar rotation which can take into account both the effect of the eccentricity of the rotating body and the perturbation by a co-orbital. By setting the mass of the co-orbital companion to zero, we retrieve the results of Colombo (1965) for a Keplerian eccentric orbit. By setting the eccentricity to zero we retrieve the results of Correia and Robutel (2013) for circular co-orbitals. We then study the rotational dynamics for eccentric co-orbitals. The case of fixed value of the eccentricities and the longitudes of the perihelion is studied section 4, while the effect of the variation of these parameters is described in section 5.

[1] http://www.minorplanetcenter.org/

2 The co-orbital dynamics

2.1 Equation of motion of the co-orbitals

We denote m_0 the mass of the central body, and m_1 and m_2 the masses of the co-orbital bodies. At order one in the eccentricity e, The variable $\zeta = \lambda_1 - \lambda_2$ satisfies the second order differential equation:

$$\ddot{\zeta} = -3\mu n^2 \left[1 - (2 - 2\cos\zeta)^{-3/2}\right] \sin\zeta \ , \tag{1}$$

with

$$\mu = \frac{m_1 + m_2}{m_0 + m_1 + m_2} \ . \tag{2}$$

This differential equation is one of the most common representations of

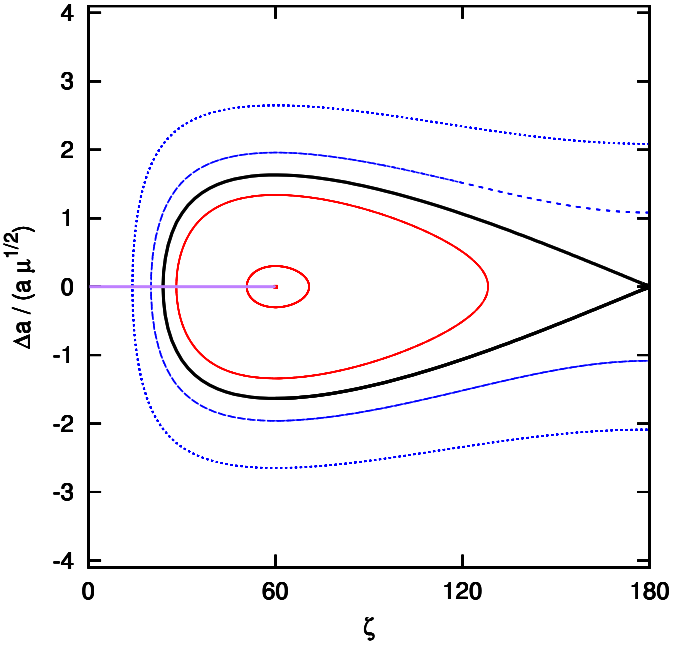

Figure 1: Phase portrait of equation (1). The vertical axis is equivalent to the variable u defined by Robutel and Pousse (2013), at the order 1 in the masses. The separatrix (black curve) splits the phase space in two different domains: inside the separatrix the region associated with the tadpole orbits (in red) and the horseshoe domain (in blue) outside. The phase portrait is symmetric with respect to $\zeta = 180°$. The horizontal purple segment indicates the range of variation of ζ_0. See the text for more details.

the coorbital motion (see Morais, 1999; Robutel et al., 2015, and references therein). It describes the relative motion of the two bodies and it is valid as long as the coorbital bodies are not too close to the collision ($\zeta = 0$).

Since equation (1) is invariant under the symmetry $\zeta \longmapsto 2\pi - \zeta$, the study of its phase portrait can be reduced to the domain $(\zeta, \dot{\zeta}) \in [0, \pi] \times \mathbb{R}$ (see Fig. 1). The equilibrium point located at $(\zeta, \dot{\zeta}) = (\pi/3, 0)$ corresponds to one of the two Lagrangian equilateral configurations[2]. In the vicinity of this equilibrium, at order one in $(\zeta - \pi/3)$, the frequency of the motion is close to (Charlier, 1906):

$$\nu = n\sqrt{\frac{27}{4}\mu}. \tag{3}$$

The other equilibrium, whose coordinates are $(\pi, 0)$, corresponds to the unstable Eulerian collinear configuration of the type L_3. The separatrices (in black in Figure 1) emanating from this last unstable point divide the phase space in three different regions: two corresponding to the tadpole trajectories surrounding one of the two Lagrange's equilibria (in red), and another corresponding to the horseshoe orbits, which encompasses the three above-mentioned fixed points (in blue). As shown in Fig. 1, any trajectory given by equation (1) can be entirely determined by the initial conditions (t_0, ζ_0) such that $\zeta(t_0) = \zeta_0$ and $\dot{\zeta}(t_0) = 0$, where ζ_0 is the minimum value of ζ along the trajectory, and t_0 the first positive instant for which the value ζ_0 is reached.

The possible values of ζ_0, represented by the purple horizontal line on Figure 1, are included in the interval $(0°, 60°]$. $\zeta_0 = 60°$ corresponds to the equilateral configuration where m_1 is the leading body and m_2 the trailing one. The tadpole orbits correspond to $\zeta_0 \in (\zeta_s, 60°]$, where $\zeta_s \approx 23.9°$ corresponds to the separatrix, while ζ_0 ranges from ζ_s to 0 for horseshoe orbits.

The expressions of λ_j and a_j, the semi-major axis of the body j, are given by (Robutel et al., 2015):

$$\lambda_j = \frac{z_0}{2} + nt + (-1)^{j+1}\frac{m_k}{m_1 + m_2}\zeta + \mathcal{O}(\mu, e\sqrt{\mu}, e^2), \quad k \neq j \tag{4}$$

and

$$a_j = \overline{a}\left(1 + (-1)^j \frac{2}{3}\frac{m_k}{m_1 + m_2}\frac{\dot{\zeta}}{n}\right) + \mathcal{O}(\mu, e\mu, e^2), \quad k \neq j, \tag{5}$$

where z_0 is a constant that is determined by the value of λ_j at $t = 0$. Using the usual expansions in eccentricity power of the distance r_j between the star and the planet j and of its true longitude f_j given by:

$$r_j = a_j\left(1 - e_j\cos(\lambda_j - \varpi_j)\right) + \mathcal{O}(e^2), \quad f_j = \lambda_j + 2e_j\sin(\lambda_j - \varpi_j) + \mathcal{O}(e^2), \tag{6}$$

[2] the coordinates of the other point are $(5\pi/3, 0)$. The permutation of the index 1 and 2 of the planets allows to exchange the two equilateral configurations, which are linearly stable for small enough planetary masses (namely, if $\frac{m_0m_1 + m_1m_2 + m_0m_2}{(m_0+m_1+m_2)^2} < \frac{1}{27} \approx 0.037$, see Gascheau, 1843).

and injecting (4) and (5) in these formulas, we get the expressions:

$$\begin{aligned} r_j &= \overline{a}\left(1 - e_j\cos(\lambda_j - \varpi_j) + (-1)^j\frac{2}{3}\frac{m_k}{m_1+m_2}\frac{\dot{\zeta}}{n}\right) + \mathcal{O}(\mu, e\mu, e^2), \\ f_j &= \lambda_j + 2e_j\sin(\lambda_j - \varpi_j) + \mathcal{O}(\mu, e\sqrt{\mu}, e^2), \end{aligned} \tag{7}$$

where λ_j is given by (4) and ζ satisfies the differential equation (1). In expressions (7), the eccentricities and the longitudes of the periastron are not necessarily constant, but their variations occur on a much longer time-scale than the one associated to the variations of ζ.

According to Robutel and Pousse (2013), in the vicinity of L_4 or L_5, the temporal variations of $X_j = e_j\exp(i\varpi_j)$ can be approximated by the expressions

$$X_1(t) = \mathrm{e}^{i\zeta_L}\left(\sqrt{\frac{m_2}{m_1}}z_1\,\mathrm{e}^{ig_1t} + z_2\,\mathrm{e}^{ig_2t}\right), \quad X_2(t) = -\sqrt{\frac{m_1}{m_2}}z_1\,\mathrm{e}^{ig_1t} + z_2\,\mathrm{e}^{ig_2t}\,. \tag{8}$$

where $\zeta_L = \pi/3$ ou $-\pi/3$ depending on the selected Lagrange configuration. The complex numbers z_1 and z_2 are two constants that can be determined by the initial values of X_1 and X_2, and g_1 and g_2 are the two eigenfrequencies of the differential system associated to the X_i. If we introduce the quantities ρ_1, ρ_2 and φ such that $z_1 = \rho_1$ and $z_2 = \rho_2\,\mathrm{e}^{i\varphi}$, the elliptic Lagrange family arises for $\rho_1 = 0$ and $\rho_2 > 0$. The two eccentricities are equal and the apsidal lines are fixed with $\varpi_1 - \varpi_2 = \zeta_L$.

At the Lagrangian points one of the eigenfrequencies vanish, since these equilibria points are degenerated. More precisely, we have:

$$g_1 = \frac{27}{8}\frac{m_1+m_2}{m_0}n, \quad g_2 = 0. \tag{9}$$

It is worth mentioning that the degeneracy is removed as soon as one moves away from the equilibrium point. Indeed, in the neighbourhood of the Lagrangian equilibrium, it can be shown that (Robutel and Pousse, 2013):

$$g_2 = \mathcal{O}\left(\frac{m_1+m_2}{m_0}\max(\zeta - \zeta_L)^2\right). \tag{10}$$

Consequently, we are left with 4 different time-scales: $2\pi/n = \mathcal{O}(1)$ associated to the orbital motions, $2\pi/\nu = \mathcal{O}(1/\sqrt{\mu})$ which governs the variations of ζ and of the semi-major axis a_j, $2\pi/g_1 = \mathcal{O}(1/\mu)$ corresponding to the secular variations of the eccentricities and ϖ_j, and $2\pi/g_2$ which is associated to the precession of the perihelion and which is the slowest one (we always have $g_2 \ll g_1$, Robutel and Pousse, 2013). In the vicinity of this configuration, for $0 < \rho_1 \ll \rho_2$, the temporal variations of e_j and ϖ_j can be

approximated by:

$$\begin{aligned} e_j &= \rho_2 \left(1 + (-1)^{j+1} \sqrt{\frac{m_k}{m_j}} \frac{\rho_1}{\rho_2} \cos(gt - \varphi) + \mathcal{O}_2\left(\frac{\rho_1}{\rho_2}\right)\right), \\ \varpi_j &\approx \delta_{j,1}\zeta_L + \varphi + g_2 t - (-1)^{j+1} \sqrt{\frac{m_k}{m_j}} \frac{\rho_1}{\rho_2} \sin(gt - \varphi) + \mathcal{O}_2\left(\frac{\rho_1}{\rho_2}\right), \end{aligned} \tag{11}$$

where $g = g_1 - g_2 \approx g_1$, and $\delta_{j,1} = 1$ if $j = 1$ and 0 otherwise. The two eccentricities are almost equal undergoing small periodic variations at the frequency g in opposition of phase. The two apsidal lines precess at a very low common frequency (and are fixed if $\zeta = \zeta_L$), and librate at the frequency g with an amplitude of $(\sqrt{m_1/m_2} + \sqrt{m_2/m_1})\rho_1\rho_2$.

3 Spin Dynamics

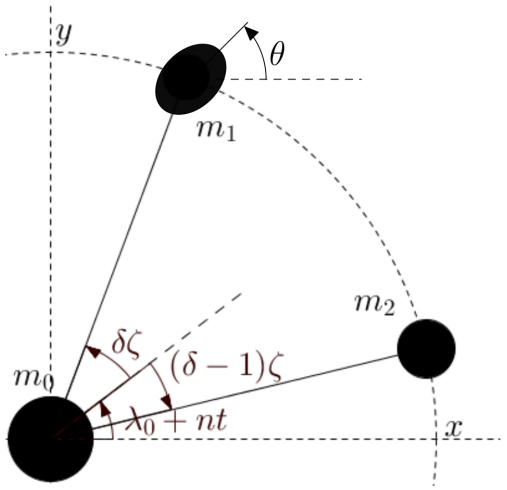

Figure 2: Reference angles represented for the circular coorbital system with respect to an inertial frame (x, y). m_0 is the mass of the central star, m_1 and m_2 the mass of the coorbitals. r_i is the distance of the coorbital i to the central star, and λ_i its true longitude. n is the mean motion of the planets' barycentre and $\zeta = \lambda_1 - \lambda_2$. Following equation (4) one can write λ_i as a function of λ_0, ζ and the mass ratio $\delta = \frac{m_2}{m_1+m_2}$. θ is the rotation angle of m_1, defined with respect to an inertial frame, that will be used in the following sections.

We focus our study in the rotation of the body 1, since the co-orbital problem is symmetric. Thus, hereafter we drop the indices 1 (r_1 becomes r etc.). We denote $A < B < C$ the moments of inertia of the rotating

body. For simplicity, we assume that the body is rotating around its main inertia axis which is held perpendicular to the orbital plane. Therefore, the rotation of the body can be described by the rotation angle θ (see Fig. 2). The equation of motion for θ is given by the canonical equations associated with the Hamiltonian $\mathcal{H}$ given by (e.g. Danby, 1964)

$$\mathcal{H} = T + \frac{I^2}{2} - \frac{\sigma^2}{4}\left(\frac{\bar{a}}{r}(t)\right)^3 \cos\ 2(\theta - f(t)), \tag{12}$$

where f is the true longitude and

$$\sigma = n\sqrt{3\frac{B-A}{C}} \tag{13}$$

is a measure of the axial asymmetry of the rotating body. This parameter is considered as constant in this study (rigid body). $(B-A)/C$ for bodies of the solar system can be found in Appendix A.

For circular unperturbed Keplerian orbits, $r = \bar{a}$ and $f = nt$, so the Hamiltonian (12) is equivalent to the equation of a simple pendulum and it is consequently integrable. The single resonant island is centred on $\dot{\theta} = n$ and the maximum width of this island (in the direction of $\dot{\theta}$) is 2σ. This resonance is called the synchronous spin-orbit resonance.

In the co-orbital eccentric case, the equations of motion are not integrable. However, an eccentric orbit perturbed by a co-orbital companion remains quasi-periodic. As a consequence, the elliptic elements of the body can be expanded in a Fourier series whose frequencies are the fundamental frequencies of the orbit (n, ν, g and g_2), see section 2. Following the D'Alembert rules, the expansion of the time-dependent quantity $\left(\frac{a}{r}\right)^3 \mathrm{e}^{i2f}$ that appears in equation (12) can be written as:

$$\left(\frac{\bar{a}}{r}\right)^3 \mathrm{e}^{i2f} = \sum_{j\geq 0} \hat{\rho}^2_{\eta_j}\ \mathrm{e}^{i(2\langle \eta_j, \varsigma\rangle t + \phi_j)}\,. \tag{14}$$

where $\varsigma = (n - g_2, \nu, g) \in \mathbb{R}^3_+$, $\eta_j = (p, q, s)$ with $2\eta_j \in \mathbb{Z}^3$, $\langle \eta_j, \varsigma\rangle = p(n - g_2) + q\nu + sg$, and $\hat{\rho}_{\eta_j} \in \mathbb{R}_+$ with:

$$\hat{\rho}^2_{\eta_j}\,\mathrm{e}^{i\phi_j} = \frac{1}{\pi}\int_0^\pi \left(\frac{\bar{a}}{r}\right)^3 \mathrm{e}^{i2(f - \langle \eta_j, \varsigma\rangle t)}\ dt\ . \tag{15}$$

Since g_2 is small with respect to the other frequencies of the system (see section 2), and have for sole effect to slightly offset the frequency n, we consider from now on that $n - g_2 \approx n$. We refer to the spin-orbit resonances located in $\dot{\theta} = pn$, i.e. those with $\eta_j = (p, 0, 0)$, as "eccentric spin-orbit resonances", and "coorbital spin-orbit resonances" those located in $\dot{\theta} = pn \pm q\nu$ ($\eta_j = (p, q, 0)_{q\neq 0}$). Replacing equation (14) into equation (12) and denoting

$\rho_{\eta_j} \equiv \sigma\hat{\rho}_{\eta_j}$, we get:

$$\mathcal{H} = T + \frac{I^2}{2} - \sum_{j\geq 0} \frac{\rho_{\eta_j}^2}{2} \cos\,(2\theta + 2\langle\eta_j, \varsigma\rangle t + \phi_j). \tag{16}$$

$\mathcal{H}$ can be seen as the Hamiltonian of a quasi-periodically perturbed pendulum, whose forcing frequencies are n, ν, g and g_2. This is a generalisation of the results by Colombo (1965) and Goldreich and Peale (1966), who showed that there is a whole family of eccentric spin-orbit resonances centred at $\dot{\theta} = pn$ in the eccentric Keplerian case. Here we have a much larger family of spin-orbit resonances centred at $\dot{\theta} = \langle\eta_j, \varsigma\rangle$ with half-width ρ_{η_j}. Since we generally have $n \gg \nu \gg g \gg g_2$, as long as $\sigma \ll n$, i.e. as long as the resonances do not overlap, it is possible to study the rotational dynamics in the vicinity of a particular eccentric spin-orbit resonance ($\dot{\theta} = pn$), because it is not perturbed by the other eccentric spin-orbit resonances. Following Goldreich and Peale (1966), one can get an approximated integrable equation for the rotation in the vicinity of $\dot{\theta} = pn$ by studying the angle γ_p, defined as:

$$\gamma_p \equiv \theta - pnt, \tag{17}$$

where p specifies the eccentric spin-orbit resonance that we are studying. For example, $p = 1$ in the case of the synchronous resonance like the case of the Moon, and $p = 3/2$ in the case of the 3:2 resonance of Mercury.

In order to adopt an autonomous Hamiltonian formulation which takes into account the different time-scales, we denote $\lambda = nt$, $\tau = \nu t$, $\upsilon = gt$ and $\upsilon_2 = g_2 t$. We recall that n is the mean mean motion of the system, $\nu = \mathcal{O}(\sqrt{\mu})$ is the fundamental frequency of the libration angle ζ, and $g = \mathcal{O}(\mu)$ and $g_2 = \mathcal{O}(\mu)$ are the frequencies of libration and precession of the pericenter, respectively. In our study we consider only slightly eccentric orbits, and $\mu \ll 1$, we can thus neglect the terms of order μ, e^2 and $\sqrt{\mu}e$ or above in the perturbation. The solution for ζ in equation (1) can be rewritten as:

$$\zeta(t) = \zeta(\tau/\nu) = \hat{\zeta}(\tau). \tag{18}$$

In the case of co-orbital bodies, at first order in eccentricity, injecting (4) into equations (7) we have:

$$f = f_0 + nt + \delta\hat{\zeta}(\tau) + 2e(\upsilon)\sin u, \tag{19}$$

with $u = \lambda - \varpi(\upsilon, \upsilon_2) + \delta\hat{\zeta}(\tau)$, $\delta = \frac{m_2}{m_1+m_2}$, and

$$\left(\frac{\bar{a}}{r}\right)^3 = 1 + h(\lambda, \tau, \upsilon) + \mathcal{O}(\mu, e\sqrt{\mu}), \tag{20}$$

where

$$h(\lambda, \tau, \upsilon) = 2\frac{\nu}{n}\delta\hat{\zeta}'(\tau) - 3e(\upsilon)\cos u. \tag{21}$$

Using the conjugated variables $(\gamma_p, \Gamma_p) = (\theta - pnt, \dot{\theta} - pn)$, (λ, Λ), (τ, T), (υ, Υ) and (υ_2, Υ_2) the Hamiltonian (12) becomes:

$$\mathcal{H} = \mathcal{H}_0 + \mathcal{H}_1 + \mathcal{O}(\mu, \sqrt{\mu}e, e^2), \tag{22}$$

with

$$\mathcal{H}_0 = n\Lambda + \nu T + g\Upsilon + g_2\Upsilon_2 + \frac{\Gamma_p^2}{2}, \tag{23}$$

and

$$\mathcal{H}_1 = -\frac{\sigma^2}{4}(1 + h(\lambda, \tau, \upsilon)) \cos 2(\gamma_p + (p-1)\lambda - \varpi(\upsilon, \upsilon_2) - \delta\hat{\zeta}(\tau) - 2e(\upsilon) \sin u). \tag{24}$$

The Hamiltonian $\mathcal{H}$ describes the motion of a rotating asymmetric body in a perturbed Keplerian orbit, at order 1 in e. As in equation (16), we can develop $\mathcal{H}$ in a Fourier series, which gives:

$$\mathcal{H} = \mathcal{H}_0 - \sum_{j \geq 0} \frac{\rho_{\eta_j}^2}{4} \cos(2\gamma_p + 2\langle \eta_j, \varsigma \rangle t + \phi_j) + \mathcal{O}(\mu, \sqrt{\mu}e, e^2). \tag{25}$$

3.1 Dynamical regimes

Following Chirikov (1979), the dynamics of the rotating body depends on the width of the resonant island ρ_{η_j} and on the distance between the center of the resonant islands. We define the distance between the center of two resonant islands as:

$$\epsilon_j^k = |\langle \eta_j - \eta_k, \varsigma \rangle|. \tag{26}$$

Chirikov's resonance overlap criterion states that when the sum of the two unperturbed half-widths is commensurate to the separation of the resonance center ($\epsilon_j^k \approx \rho_{\eta_j} + \rho_{\eta_k}$), large-scale chaos ensues (Chirikov (1979); Murray and Dermott (1999)) as it is the case for the rotation of Hyperion (Wisdom et al. (1984b)) in the eccentric Keplerian case.

When $(\rho_{\eta_j} + \rho_{\eta_k}) \ll \epsilon_j^k$ the islands are isolated and only small areas near the separatrix of the pendulums are chaotic. Most of the trajectories between those island are quasi-periodic. If we consider a weak dissipation, the rotation can be captured in one of those resonances. The wider the resonant island is, the higher are the probabilities of being captured in it (Goldreich and Peale (1966)).

Finally if $(\rho_{\eta_j} + \rho_{\eta_k}) \gg \epsilon_j^k$, resonant islands totally overlap and we get the dynamics of a modulated pendulum (see Morbidelli, 2002, page 222). This situation is likely to occur when the Keplerian motion is perturbed by secular phenomena, for example by the precession of the orbits in the planetary case.

In the co-orbital case, the libration is on a semi-secular time scale. Let us consider two resonances separated by $\epsilon_j^k = \nu/2$ (for example $\eta_j = (1, 1/2, 0)$

and $\eta_k = (1, 0, 0)$). As we will see in the following sections, $\rho_{\eta_j}/\sigma \leq 1$, thus $(\rho_{\eta_j} + \rho_{\eta_k}) < 2\sigma$. In general, we have $\sigma/n < 1$ and $\nu/n \leq 0.1$, depending on μ and ζ_0 (Leleu et al., 2015). As a consequence, the resonant islands of two resonances separated by $\epsilon_j^k = \nu/2$ can either be isolated, overlapping, or simply reduced to a single modulated resonance, depending on the values of ρ_{η_j} and ν. Our purpose is thus to estimate the width of the spin-orbit resonances induced by the orbital frequencies n, ν and g.

3.2 Unperturbed Keplerian Orbits

One can obtain the Hamiltonian for the rotation of an asymmetric body on a single Keplerian orbit by simplifying the Hamiltonian $\mathcal{H}$ (Eq. 22). Indeed, by taking the mass of the perturbing body equal to 0 ($\delta = 0$), we obtain

$$\mathcal{H}_K = \mathcal{H}_0 - \frac{\sigma^2}{4}(1 - 3e\cos\lambda)\cos 2(\gamma_p + (p-1)\lambda - 2e\sin\lambda) + \mathcal{O}(e^2). \quad (27)$$

In order to study the spin dynamics near a specific eccentric spin-orbit resonance, we can fix p. We can thus write $\mathcal{H}_K$ as:

$$\mathcal{H}_K = \mathcal{H}_0(\Gamma_p, \Lambda) + \mathcal{H}_{1,p}(\gamma_p, \lambda) + \mathcal{O}(e^2), \quad (28)$$

with $\mathcal{H}_{1,p}$ a periodic function of λ. We can thus develop $\mathcal{H}_{1,p}$ as a Fourier series:

$$\mathcal{H}_{1,p}(\gamma_p, \lambda) = \overline{\mathcal{H}}_{1,p}(\gamma_p) + \sum_{k\neq 0} C_k(\gamma_p)\cos(k\lambda), \quad (29)$$

with k an integer, and

$$\overline{\mathcal{H}}_{1,p} = -\frac{\sigma^2}{4} X_p^{-3,2}(e)\cos 2\gamma_p + \mathcal{O}(e^2). \quad (30)$$

$X_p^{-3,2}(e) = \mathcal{O}(e^{2|p-1|})$ are the Hansen coefficients , given by:

$$\left(\frac{r}{a}\right)^{k_1} \mathrm{e}^{ik_2 f} = \sum_{2p\in\mathbb{Z}} X_p^{k_1,k_2}\, \mathrm{e}^{i2pM} \quad (31)$$

where M is the mean anomaly of the rotating body (Hansen, 1855). As we limited our description to the first order of eccentricity, only three of the first order resonances have no-null coefficients: $X_1^{-3,2}(e) = 1 + \mathcal{O}(e^2)$, $X_{1/2}^{-3,2}(e) = -\frac{e}{2} + \mathcal{O}(e^2)$ and $X_{3/2}^{-3,2}(e) = \frac{7e}{2} + \mathcal{O}(e^2)$.

For each individual eccentric resonances, we have $|\dot{\gamma}_p| \ll n$. We can thus average $\mathcal{H}_K$ over λ to get

$$\overline{\mathcal{H}}_K = \mathcal{H}_0(\Gamma_p, \Lambda, T) + \overline{\mathcal{H}}_{1,p}(\gamma_p) + \mathcal{O}(e^2). \quad (32)$$

We can recognize in the expression of $\overline{\mathcal{H}}_K$ the first terms of the family of the eccentric spin-orbit resonances located in $\dot{\theta} = pn$ (Goldreich and Peale (1966)). For these resonances, we have $\rho_{(p,0,0)} = \sigma\sqrt{|X_p^{-3,2}(e)|}$.

4 Coorbital bodies with constant eccentricity

We now consider the co-orbital perturbations on a eccentric Keplerian orbit, for which e and ϖ can be considered as constant, either because their variations are too slow ($g = \mathcal{O}(\mu)$), or because the amplitude of these variations can be neglected. We thus consider only the sets $\eta_j = (p, q, 0) = (p, q)$. Let us express the equation of rotation (12) as a function of γ_p and ζ. Taking $\varpi = 0$, $\mathcal{H}_1$ (equation (24)) becomes:

$$\mathcal{H}_1 = -\frac{\sigma^2}{4}(1 + h(\lambda, \tau)) \cos 2(\gamma_p + (p-1)\lambda - \delta\hat{\zeta}(\tau) - 2e \sin u), \tag{33}$$

where

$$h(\lambda, \tau) = \frac{2\nu\delta\hat{\zeta}'(\tau)}{n} - 3e\cos(\lambda + \delta\hat{\zeta}(\tau)). \tag{34}$$

Similarly to the Keplerian case, at order one in e we can chose $p \in \{1/2, 1, 3/2\}$ and average $\mathcal{H}_1$ over λ, obtaining:

$$\overline{\mathcal{H}}_{1,p} = -\frac{\sigma^2}{4}[X_p^{-3,2}(e) + H_c(p)] \cos(2\gamma_p - 2p\hat{\zeta}(\tau)), \tag{35}$$

where the Hansen coefficients $X_p^{-3,2}(e)$ are identical to the Keplerian case, $H_c(1) = -\frac{2\delta\nu\hat{\zeta}'}{n}$ and $H_c(1/2) = H_c(3/2) = 0$.

Equation (1) is not integrable, so in general we cannot obtain an analytical expression of the ρ_{η_j} in the co-orbital case. Nevertheless, when ζ_0 is near to the Lagrangian equilibrium ζ_L, we can find a simple approximate expression for ζ, and express the ρ_{η_j} as functions of the initial parameters.

4.1 Near the Lagrangian Circular Equilibrium

We use a development of order 2 to understand the behaviour of the system for ζ_0 near ζ_L, *i.e.*, in the vicinity the Lagrangian circular equilibrium point (we recall that ζ_0 is the minimal value reached by $\zeta(t) = \lambda_1(t) - \lambda_2(t)$ during a libration period, and $\zeta_L = \pi/3$ for the l_4 equilibrium and $5\pi/3$ for the l_5 one). We define $z = \zeta_0 - \zeta_L$, the departure from the Lagrangian equilibrium at $t = 0$ and $\frac{d\hat{\zeta}}{d\tau} = 0$. A quadratic approximation of the solution of the equation (1) is:

$$\hat{\zeta}(\tau) = \zeta_L + \frac{3\sqrt{3}}{8}z^2 + (1 - \frac{\sqrt{3}}{4}z)z\cos(\tau) - \frac{\sqrt{3}}{8}z^2\cos(2\tau) + \mathcal{O}(z^3). \tag{36}$$

The constant term $\zeta_L + \frac{3\sqrt{3}}{8}z^2$ can be absorbed by a redefinition of λ and γ_p, we thus neglect it from now on. At second order in z, the averaged part

of the Hamiltonian $\overline{\mathcal{H}}_{1,p}$, equation (35), becomes, for $p = 1$:

$$\begin{aligned}\overline{\mathcal{H}}_{1,p=1} = -\frac{\sigma^2}{4}\Bigg[&(1-z^2\delta^2)\cos(2\gamma_1) + z\delta(1-\frac{\sqrt{3}}{4}z-\frac{\nu}{n})\cos(2\gamma_1+\tau-\frac{\pi}{2})\\ &+z\delta(1-\frac{\sqrt{3}}{4}z+\frac{\nu}{n})\cos(2\gamma_1-\tau-\frac{\pi}{2})\\ &+\frac{z^2\delta}{2}\sqrt{\delta^2+\frac{3}{16}}\cos(2\gamma_1+2\tau+\phi)\\ &+\frac{z^2\delta}{2}\sqrt{\delta^2+\frac{3}{16}}\cos(2\gamma_1-2\tau+\phi)\Bigg] + \mathcal{O}(e^2, ez^2, z\mu),\end{aligned} \tag{37}$$

with ϕ a phase depending on z and $\delta = m_2/(m_1+m_2)$, and for $p = 3/2$ or $1/2$:

$$\begin{aligned}\overline{\mathcal{H}}_{1,p} = -\frac{\sigma^2}{4}X_p^{-3,2}(e)\,&[\cos(2\gamma_p) + pz\delta\cos(2\gamma_p+\tau)\\ &+pz\delta\cos(2\gamma_p-\tau)] + \mathcal{O}(e^2, ez^2, z\mu).\end{aligned} \tag{38}$$

First, let us consider these results at first order in e and z. If $e = 0$, we get the expression in the quasi-circular case, as developed by Correia and Robutel (2013). In that paper, the authors studied the overlap between the synchronous resonant island $\eta_j = (1, 0)$ and the island centred at $\eta_j = (1, \pm 1/2)$. Here we generalise the study to the vicinity of the eccentric spin-orbit resonances $\eta_j = (1/2, 0)$ and $\eta_j = (3/2, 0)$.

In the unperturbed eccentric case, we recalled in the previous section that there were eccentric spin-orbit resonances centred at $\eta_j = (p, 0)_{p\in\{1/2,1,3/2\}}$. The libration of amplitude z around the Lagrangian equilibrium splits each of these eccentric resonances into three resonant islands as well. Equation (38) shows that we can approximate the phase portrait in the vicinity of each of the unperturbed eccentric spin-orbit resonances (1:1, 3:2 or 1:2) by an island of half-width $\rho_{(p,0)} = \sqrt{X_p^{-3,2}(e)}\sigma$ centred at $\eta_j = (p, 0)$ and two island of half-width $\rho_{(p,\pm 1/2)} = \sqrt{pz\delta X_p^{-3,2}(e)}\sigma$ located at $\eta_j = (p, \pm 1/2)$ (see Figure 5). The contribution of $\hat{\zeta}'$ in the expression of h (equation (34)) is of order $\nu/n = \mathcal{O}(\sqrt{\mu})$, and we will neglect it from now on.

We can estimate for which values of the axial asymmetry of the rotation body σ the resonant islands in $\eta_j = (p, 0)$ and $\eta_k = (p, -1/2)$ begin to overlap. We recall that near the Lagrangian equilibrium, $\nu = n\sqrt{27\mu}/2$. Therefore, for these resonances $\epsilon_j^k = n\sqrt{27\mu}/4$ and $(\rho_{\eta_j} + \rho_{\eta_k}) = (1 + \sqrt{z\delta})\sigma\sqrt{X_p^{-3,2}(e)}$. By using the definition of σ (equation (13)), one can

see that these resonant islands overlap when

$$\frac{B-A}{C} \approx \frac{9}{16\sqrt{X_p^{-3,2}(e)}}(1-2\sqrt{z\delta})\mu \ . \tag{39}$$

The interaction between two islands of first order in z is also theoretically possible, for example the islands $\eta_j = (1, 1/2)$ and $\eta_k = (3/2, -1/2)$ (see Figure 6). However, in order to get those two islands near to each other, we need to have $\nu \approx n/2$, which is near the stability limit $\nu = n/\sqrt{2}$ given by Gascheau (1843). Moreover, in order to interact, these two islands also need to present large libration widths, but a simultaneously large amplitude z and a high frequency ν is not possible for stability reasons (Leleu et al., 2015).

Due to the truncation of the terms of order ez^2, only the synchronous resonance is modified by the terms in z^2 in this model. For large libration amplitudes z, co-orbital resonant islands of width proportional to z^2 appear in $\dot{\theta} = n \pm \nu$, while the width of the synchronous island decreases (see Fig 4 and 5). In next section we will see that the trends of the quadratic model are confirmed for larger libration amplitudes, and a similar behaviour occurs in the vicinity of all eccentric spin-orbit resonances.

4.2 Tadpole and Horseshoe Configurations

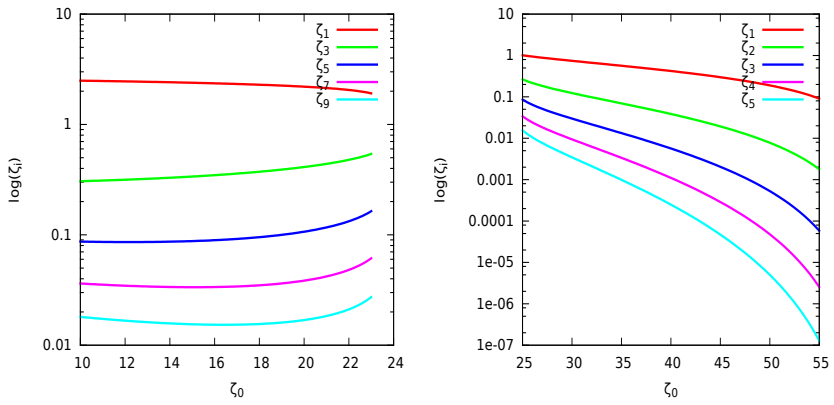

Figure 3: The five dominant coefficients of the Fourier expansion of $\hat{\zeta}$, equation (41). The ξ_l have been obtained by a numerical integration of equation (1) followed by a frequency analysis. They depend only on ζ_0. On the left, in the horseshoe case, the symmetry of the orbit imposes that $\xi_{2l} = 0$ (Robutel et al., 2012). On the right, we represented those coefficients for the tadpole configuration.

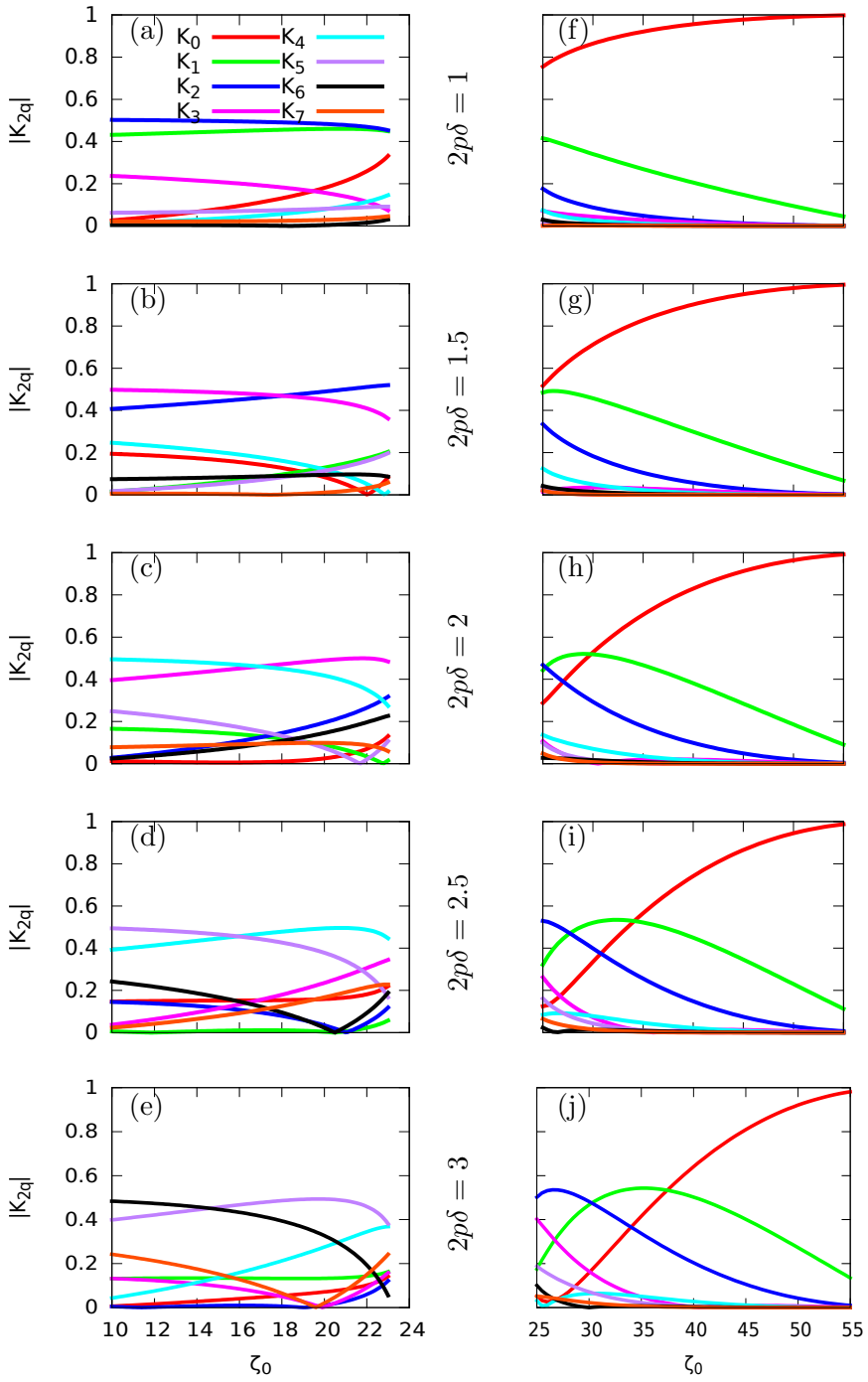

Figure 4: The seven firsts $|K_{2q}|_{2q\in\mathbb{Z}}$ coefficients with respect to ζ_0 for the horseshoe on the left and for the tadpole orbits orbits on the right. For (a) & (f) we have $2p\delta = 1$, for (b) & (g) $2p\delta = 3/2$, for (c) & (h) $2p\delta = 2$, for (d) & (i) $2p\delta = 5/2$ and for (e) & (j) $2p\delta = 3$. see the text for more details.

We now describe the spin dynamics of the coorbital in the whole tadpole and horseshoe domains. To do so, we write the averaged part of the Hamiltonian $\overline{\mathcal{H}}_p$ (35) under the form:

$$\overline{\mathcal{H}}_p = \mathcal{H}_0 - \sum_{q\in\mathbb{Z}} \frac{\rho^2_{(p,q)}}{4} \cos(2\gamma_p + q\tau + \phi), \tag{40}$$

The explicit expression of this Hamiltonian given in section 4.1 is no more valid for $\zeta_0 - \zeta_L \gg 1$. In order to have a valid expression everywhere in the tadpole and horseshoe domain, we consider the fourier expansion of the solution $\hat{\zeta}(\tau)$ of equation (35). $\hat{\zeta}$ being a real function of period 2π, we can write:

$$\hat{\zeta} = \xi_0 + \sum_{l\geq 1} \xi_l \sin(l\tau + \varphi_l) \tag{41}$$

The coefficients ξ_l can be obtained numerically. In Figure 3 we show the evolution of the lower order ξ_l with respect to ζ_0. Replacing equation (41) into (35) and neglecting the terms of order $\sqrt{\mu}$ (see section 4.1), we can write:

$$\overline{\mathcal{H}}_{1,p} = -\frac{\sigma^2}{4} X_p^{-3,2}(e) \Re(\mathrm{e}^{i2\gamma_p}\, \mathrm{e}^{-i2p\delta\hat{\zeta}(\tau)}). \tag{42}$$

Since $\mathrm{e}^{-i2p\delta\hat{\zeta}(\tau)}$ is a periodic function with period 2π in τ, we can also expand it in Fourier series[3]

$$\mathrm{e}^{-i2p\delta\hat{\zeta}(\tau)} = \sum_{2q\in\mathbb{Z}} K_{2q}(p\delta,\zeta_0)\, \mathrm{e}^{i(2q\tau+\Phi^p_{2q})} \ , \tag{43}$$

and thus rewrite equation (42) as

$$\overline{\mathcal{H}}_{1,p} = -\frac{\sigma^2}{4} X_p^{-3,2}(e) \sum_{2q\in\mathbb{Z}} K_{2q}(p\delta,\zeta_0) \cos(2\gamma_p + 2q\tau + \phi) \ . \tag{44}$$

By determining the K_{2q} coefficients, we can thus directly obtain the ρ_{η_j} from

$$\rho_{(p,q)} = \sigma\sqrt{X_p^{-3,2}(e) K_{2q}(p\delta,\zeta_0)} \ . \tag{45}$$

The coefficients K_{2q} are a function of the ξ_l appearing in eq. (41). Replacing equation (41) into $\mathrm{e}^{-i2p\delta\hat{\zeta}(\tau)}$ gives

$$\mathrm{e}^{-i2p\delta\hat{\zeta}(\tau)} = \mathrm{e}^{-i2p\delta\xi_0}\, \mathrm{e}^{-i2p\delta\sum_{l\geq 0}\xi_l \sin(l\tau+\phi_l)} \ , \tag{46}$$

and thus

$$\mathrm{e}^{-i2p\delta\hat{\zeta}(\tau)} = \mathrm{e}^{-i2p\delta\xi_0} \prod_{l\geq 1} \mathrm{e}^{-i2p\delta\xi_l \sin(l\tau+\phi_l)} \ . \tag{47}$$

[3]Note that since ξ_l depends only on ζ_0, the coefficients K_q depend only on the product $p\delta$ instead of p and δ.

By using the Bessel functions, we can further write:

$$\mathrm{e}^{-i2p\delta\hat{\zeta}(\tau)} = \mathrm{e}^{-i2p\delta\xi_0} \prod_{l\geq 1} \sum_{k\in\mathbb{Z}} J_k(-2p\delta\xi_l)\ \mathrm{e}^{ik(l\tau+\phi_l)}\,. \tag{48}$$

where J_k is the k^{th} bessel function. Replacing this last expression into the equation (42), we get:

$$K_{2q}(p\delta,\zeta_0) = \prod_{j=1}^{\infty} J_{k_j}(-2p\delta\xi_j(\zeta_0)), \quad \text{with } (k_1,k_2,..,k_j,..) \,/\, \sum_{j=1}^{\infty} jk_j = 2q. \tag{49}$$

We finally obtain an expression for the $\rho_{(p,q)}$ through expression (45), which depends on the ξ_l (Eq. 41). Recalling the propriety of the Bessel function $j_{-k} = (-1)^k J_k$, we have $|K_{-2q}| = |K_{2q}|$.

In Figure 4 we plot several $K_{2q}(p\delta,\zeta_0)$ coefficients as a function of ζ_0 for different values of $p\delta$. The ξ_l coefficients are obtained by integration of equation (1) followed by a frequency analysis of the solution with a truncation at $l = 10$ (see the exponential decreasing of the ξ_l in l, Fig. 3). The fact that the coefficients K_{2q} depend only on p and δ by the product $p\delta$ yields an interesting result: the relative width of the resonant islands in the vicinity of the 1/2 resonance in the restricted case ($\delta = m_2/(m_1+m_2) \approx 1$) and in the vicinity of the 1:1 resonance with equal masses ($\delta = 1/2$) are identical within our approximations, since in both case $2p\delta = 1$. However, the width ρ_j of these islands differ because the Hansen coefficients $X_p^{-3,2}(e)$ depend on p.

The amplitude of the K_{2q} in Fig. 4 indicates which resonant island is dominating in the vicinity of a given spin-orbit resonance. In the tadpole cases (panels a to e), we have most of the time a phase portrait similar to the one in the quasi-circular case (Correia and Robutel, 2013), or the one near the elliptic Lagrangian equilibrium (section 4.1), i.e., a dominating island at $\eta_j = (p, 0)$ and smaller islands at $\eta_j = (p, \pm q)$, whose width decreases as q increases. The phase portrait of such case can be seen on Fig. 5 (left). Still in the tadpole configuration, far from the Lagrangian equilibrium, several resonant island may become of commensurable width. An example of this is shown in the right panel of the Figure 5, which corresponds to the same case shown in Fig. 4 (b) for $\zeta_0 = 25°$. For high values of the product $p\delta$ and far from the Lagrangian equilibrium, the width of the island centred at $\eta_j = (p, 0)$ can even been small with respect to the island located in $q = 1/2$ or $q = 1$ (see for example Fig. 4 (e) for $\zeta_0 = 25°$). In the horseshoe configuration, the width of the eccentric spin-orbit resonance is always negligible with respect to the dominating islands at its vicinity. The largest islands are usually located in $\eta_j = (p, \pm q)$, with q different from zero. As the product $p\delta$ increase, the islands further away from the eccentric resonance (thus for higher q) become dominating.

As a result, the spin dynamics in the vicinity of $\eta_j = (p, 0)$ is very different between tadpole and horseshoe orbits. In the tadpole configuration, the main resonant island is generally near the eccentric resonance, forming a large chaotic area centred at $\eta_j = (p, 0)$ in the case of an overlap (Correia and Robutel, 2013). In the horseshoe case, the direct vicinity of the resonance $\eta_j = (p, 0)$ is generally regular. In case of overlapping, chaotic areas arise from each side of $\eta_j = (p, 0)$, at a distance which increases with the product $p\delta$.

The overlapping of the resonant island can change the phase portrait of the rotation from separated resonant islands to chaotic rotation and even to a simple modulation of the islands of the unperturbed Keplerian case. Now that we have an expression of the width of the resonant islands centred at $\eta_j = (p, q)$, we can identify which parameters can give rise to a chaotic behaviour. Departing from a given system, there are two ways to increase the overlap of close-in resonances:

1) widen the resonant islands: by increasing δ; by increasing the asymmetry $(\frac{B-A}{C})$ of the rotating body; by increasing e, which widens all the islands located at $\eta_j = (p, q)_{p\neq 1}$.

2) bring the resonant islands closer from each other: ν is reduced when μ decreases, since ν is proportional to $\sqrt{\mu}$ (equation 3).

Reducing ζ_0 has the double effect to widen the $\eta_j = (p, q)_{q\neq 0}$ island in one hand, and to reduce ν and thus bring the islands closer, on the other hand.

4.3 Numerical simulations

For a global view of the rotational dynamics we can use the Frequency Map Analysis (FMA) to represent the phase space (Laskar, 1993; Robutel and Laskar, 2001). This method is particularly adapted to our problem because the trajectories of the considered systems are close to quasi-periodic trajectories and their dynamics involve up to three fundamental frequencies (n, ν and g), so we cannot use Poincaré sections.

In Figure 5 we plot one of these maps for the 3:2 resonance. The vertical axis shows $\dot{\theta}/n$, such that the center of the 3:2 resonance can be found at $\dot{\theta}/n = 1.5$. The horizontal axis is $\gamma = \gamma_1$ modulo $\left[-\frac{\pi}{2}, \frac{\pi}{2}\right]$. The range of γ can be reduced to this interval due to the symmetries of the body. The purpose of these simulations is to describe the phase space ($\dot{\theta}/n$,γ) in order to identify the areas where γ librates, circulates or has a chaotic evolution. Each pixel corresponds to an initial condition in ($\dot{\theta}/n$,γ) for witch the system is integrated using equation (12) for the rotational motion together with the equations for the planar three-body problem in heliocentric coordinates. The simulations are run over several times the longest time scale considered in the system, generally $\mathcal{O}(2\pi/\nu)$ or $\mathcal{O}(2\pi/g)$ (hence $\propto 1/\sqrt{\mu}$ or $\propto 1/\mu$ orbital periods, respectively). For each of those simulations, the main frequency f

of $e^{i\gamma}$ has been computed (see Robutel et al., 2012). The color of each pixel represents the first derivative of this frequency with respect to $\dot{\theta}$, i.e., $df/d\dot{\theta}$. In the circulation region, f evolves almost linearly with respect to $\dot{\theta}$, thus the value of the derivative is almost constant. Inside the libration island, f is a constant, thus its derivative is equal to zero. Finally, at the separatrix between circulation and libration, and in the chaotic region, f is singular and so is its derivative.

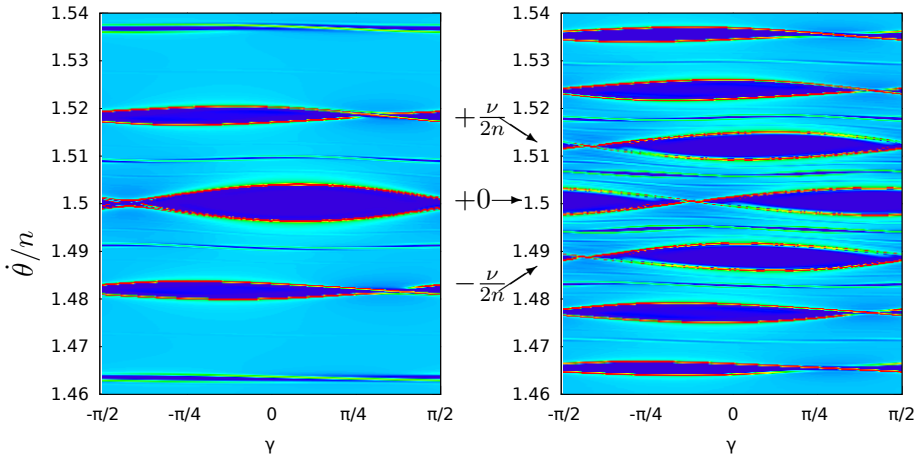

Figure 5: FMA of the phase space $(\dot{\theta}/n, \gamma_p)$ for two coorbitals in tadpole configurations. In both cases $m_1 = m_2 = 1 \times 10^{-4}\, m_0$, $e_1 = e_2 = 0.1$, and $\frac{B-A}{C} = 2 \times 10^{-5}$. Looking at the vicinity of the 3:2 eccentric spin-obit resonance, we have $2p\delta = 1.5$. On the left, we have $\zeta_0 = 45°$, $\frac{\nu}{2n} \approx 0.018$, the islands are thus located at $\dot{\theta}/n = 1.5 \pm 0.018$. On the right: $\zeta_0 = 25°$, $\nu/(2n) \approx 0.011$, the islands are thus located at $\dot{\theta}/n = 1.5 \pm 0.011$. $(B-A)/C$ for bodies of the solar system can be found in Appendix A, Table 2.

4.3.1 Tadpole orbits

We recall that a system is in a tadpole configuration when $\zeta_0 \in (\zeta_s, \zeta_L]$. We saw previously in the quadratic approximation (sections 4.1 and 4.2) that for ζ_0 close to ζ_L, the eccentric spin-orbit resonance ($\eta_j = (p, 0)$) is larger than the co-orbital resonances $\eta_j = (p, q)_{q\neq 0}$ (see Fig. 5, left panel). Far from the Lagrangian equilibrium, (and especially for high values of $2p\delta$), the width of the resonances $\eta_j = (p, \pm 1/2)$ and $\eta_j = (p, \pm 1)$ (island centred at $\dot{\theta} = pn \pm \nu/2$ or $\dot{\theta} = pn \pm \nu$, respectively) can be as wide as the eccentric islands or even larger (see Fig. 4 and Fig. 5, right). Increasing the amplitude of libration gives also rise to higher order resonant island, in-between the previously described resonant island. The appearance of such islands can

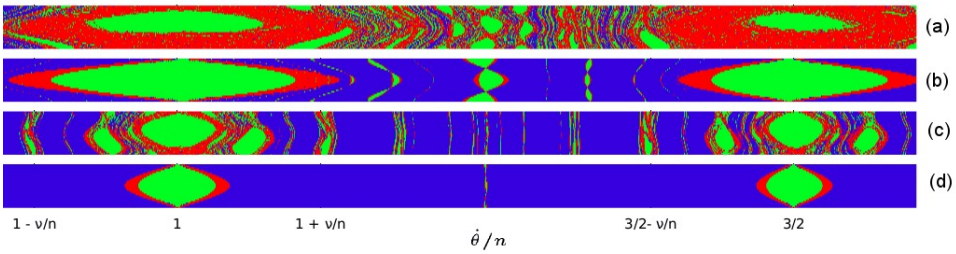

Figure 6: Frequency map of focused on the 1:1 to 3:2 resonances area. (a) and (c) represent a co-orbital configuration with $\delta = 1/2$ $\mu = 2 \times 10^{-3}$, $e = 0.15$ and $\zeta_0 = 45°$. For comparison, (b) and (d) represent the keplerian case ($\delta = 0$). $\frac{B-A}{C} = 5 \times 10^{-4}$ for (c) and (d) and $\frac{B-A}{C} = 5 \times 10^{-3}$ for (a) and (b). Blue when γ circulate, green when it is trapped in a spin-orbit resonance and red when the rotation is chaotic. See the text for more details.

accelerate the transition to a chaotic phase portrait.

For unperturbed Keplerian orbits, chaotic rotation emerges when e and σ are large enough, as it is the case for Hyperion (Wisdom et al., 1984b). However, in the co-orbital case, the generalised chaos may have a different origin. In Figure 6 (b) and (d), we show the classic eccentric resonances described in section 3.2 for unperturbed Keplerian orbits. In this plot higher order resonances in e are also visible (for example $\dot{\theta}/n = 5/4$). In Figure 6 (a) and (c) we show the previous two orbits while perturbed by a coorbital companion. We observe that each member of the eccentric spin-orbit family, including the ones of higher order than one in e, give rise to co-orbital spin orbit resonances, fulfilling the phase space and potentially overlapping each other. Moreover, generalised chaotic rotation can be reached for lower values of σ in the co-orbital case than in the unperturbed Keplerian case. This is due to a much more populated phase space, ensuring the overlap of all the resonant islands between the 1:1 and the 3:2 resonances.

4.3.2 Horseshoe orbits

For horseshoe orbits ($\zeta_0 \in (0, \zeta_s)$), the phase portrait is different from tadpole orbits. In Figure 7 we look at the vicinity of the synchronous resonance $\eta_j = (1, 0)$, in a case where $m_1 \ll m_2$. As explained in section 4.2, in the horseshoe configuration the main resonant island is not centred at the synchronous resonance, but on each side, symmetrically with respect to $\eta_j = (1, 0)$. In this case, we have $2p\delta = 2$ and $\zeta_0 = 12°$, so the main resonances are for $2q = 3$ and $2q = 4$ (see Fig. 4 h), which are centred at $\eta_j = (1, \pm 3/2)$ and $\eta_j = (1, \pm 2)$. In Figure 7 these resonances overlap, creating a chaotic area that encompass nearby resonances.

As for the synchronous resonance, in the vicinity of an eccentric spin-

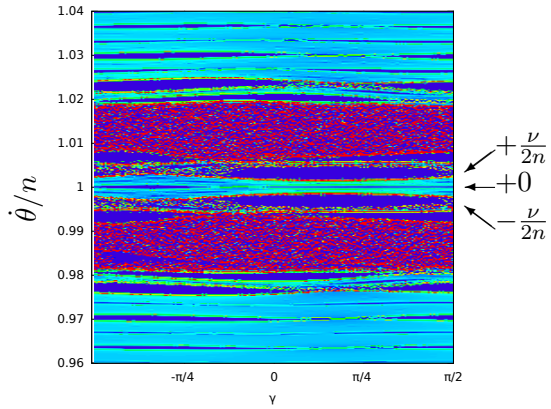

Figure 7: FMA of the phase space $(\dot{\theta}/n, \gamma_p)$ for two coorbitals on horseshoe configuration. $e_1 = e_2 = 0.1$, $\frac{B-A}{C} = 1 \times 10^{-5}$. $\zeta_0 = 12°$, $m_1 = 1 \times 10^{-7} m_0$ and $m_2 = 1 \times 10^{-5} m_0$. We focus here on the synchronous resonance with $2p\delta = 2$. $\nu/(2n) \approx 0.0033$, the islands are thus located at $\dot{\theta}/n = 1 \pm k \times 0.0033$, with k an integer.

orbit resonance ($\eta_j = (p, 0)_{p \neq 0}$), the main resonant island is not the eccentric resonance itself, since the order q of the dominating harmonics depends mainly on the product $2p\delta$. In Figure 8 we look at the vicinity of the 3:2 eccentric spin-orbit resonance for two different values of δ. On the left panel, the two coorbital have the same mass, while on the right, we are in the restricted case $m_1 \ll m_2$. We thus have $2p\delta = 3/2$ on the left and $2p\delta = 3$ on the right. Accordingly to the graphs (g) and (j) of Fig. 4, the largest resonant islands are located at $\eta_j = (3/2, \pm 1)$ and $\eta_j = (3/2, \pm 3/2)$ for the equal masses and $\eta_j = (3/2, \pm 5/2)$ and $\eta_j = (3/2, \pm 3)$ in the restricted case. It is indeed what we observe on Figure 8. In both cases, the main resonant islands overlap, creating two chaotic area symmetric with respect to the eccentric spin-orbit resonance $\eta_j = (3/2, 0)$.

Overall, In the horseshoe domain, the eccentric spin-orbit resonances are of negligible width with respect to some of the co-orbital resonant islands under and above them. In addition, since horseshoe co-orbitals are stable only for $\mu < 2 \times 10^{-4}$, the resonant island are generally closer to each other than in the tadpole configuration ($\nu = \mathcal{O}(\sqrt{\mu})$). That is why, in the three examples we have chosen, the main resonant islands always overlap.

4.3.3 Quasi satellite

Although our model does not apply to the quasi-satellite case, they have a similar dynamics near the main eccentric spin-orbit resonances. i.e. resonant islands located in $\dot{\theta} = n \pm \nu/2$. In Figure 9 we show the vicinity of the 1:1

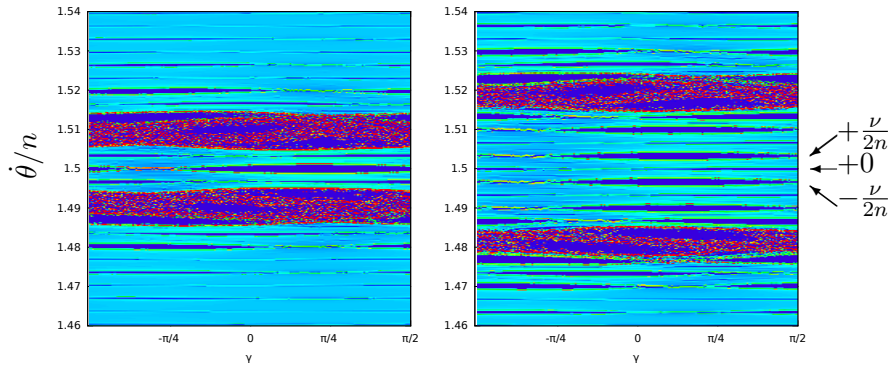

Figure 8: FMA of the phase space $(\dot{\theta}/n, \gamma_p)$ in the neighbourhood of the 3:2 spin-orbit resonance for two coorbitals on horseshoe configuration. $e_1 = e_2 = 0.1$, $\frac{B-A}{C} = 1 \times 10^{-5}$. $\zeta_0 = 12°$ in both cases. On the left we have $m_1 = m_2 = 5 \times 10^{-6} m_0$ $(2p\delta = 3/2)$. On the right we have $m_1 = 1 \times 10^{-7} m_0$, $m_2 = 1 \times 10^{-5} m_0$ $(2p\delta = 3)$. $\nu/(2n) \approx 0.0033$, the islands are thus located at $\dot{\theta}/n = 1.5 \pm k \times 0.0033$, with k an integer. See the text for more details.

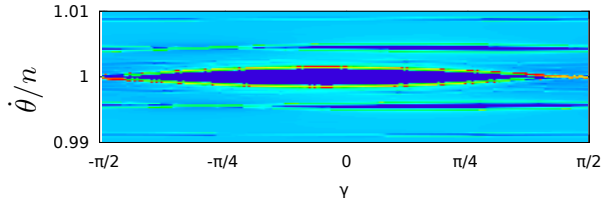

Figure 9: FMA of the phase space $(\dot{\theta}/n, \gamma_p)$ for two coorbitals in quasi-satellite configuration, near the synchronous resonance. $m_1 = m_2 = 1 \times 10^{-6} m_0$, $e_1 = e_2 = 0.2$, $\frac{B-A}{C} = 1 \times 10^{-6}$, $\varpi_1 - \varpi_2 = 180°$ and $\zeta_0 = 15°$. See the text for more details.

resonance for a quasi-satellite case. In this case $\nu/(2n) = 4.3 \times 10^{-3}$, thus the islands are located in $\dot{\theta}/n = 1 \pm \nu/(4\pi) = 1 \pm 0.0043$.

5 Coorbital bodies with variable eccentricity

Until now, we have been considering that e and ϖ are constant because either their variations are too small, either they are slow with respect to the considered time-scale. In general, the temporal evolution of e and ϖ depends on g and g_2. In the vicinity of the Lagrangian equilibrium, i.e., when the

variations of e are small, we can make the following approximation (Eq. 11):

$$e = e_0 + \Delta e \cos(gt) \ , \tag{50}$$

and

$$\varpi = \varpi_0 + w \sin(gt) + g_2 t \ . \tag{51}$$

As explained in section 3, we can neglect the effect of g_2 on the spin dynamics. The value of Δe increases when the difference between the initial eccentricities of the orbits of the co-orbital bodies also increases (see Nauenberg, 2002). In addition, Δe also increases when δ tends to 1 ($m_1 \ll m_2$). We now head back to the general form of the Hamiltonian $\mathcal{H}$ developed in section 3. By replacing the orbital variations given by expressions (50) and (51) in equation (24), we obtain a Hamiltonian that takes into account the variations of e and ϖ. At first order in w and Δe, following the method described in sections 3.2 and 4, we can split $\mathcal{H}_1$ into a term which does not depend on λ and a term that has zero as mean value over λ. After averaging, for $p = 1$, $\overline{\mathcal{H}}_{1,p}$ becomes:

$$\overline{\mathcal{H}}_{1,p=1} = -\frac{\sigma^2}{4} \cos(2\gamma_1 - 2\delta\hat{\zeta}(\tau)) \ , \tag{52}$$

while for $p = 3/2$ or $1/2$ we have

$$\begin{aligned} \overline{\mathcal{H}}_{1,p} = -\frac{\sigma^2}{4} \quad & \Big[X_p^{-3,2}(e_0) \cos(2\gamma_p - 2p\delta\hat{\zeta}(\tau)) \\ & + X_p^{-3,2}(\frac{\Delta e + we_0}{2}) \cos(2\gamma_p - 2p\delta\hat{\zeta}(\tau) + gt) \\ & + X_p^{-3,2}(\frac{\Delta e - we_0}{2}) \cos(2\gamma_p - 2p\delta\hat{\zeta}(\tau) - gt) \Big] \ . \end{aligned} \tag{53}$$

As in the cases previously studied, the rotational dynamics in the vicinity of the synchronous resonance remains unchanged by the eccentricity variations at first order in Δe and w. However, the dynamics in the vicinity of the remaining eccentric spin-orbit resonances is modified by the variations of e and ϖ. We define $\gamma_{p,\pm g} \equiv \gamma_p \pm gt$. Then, each term of the equation (53) can be rewritten under the form of the equation (35). As a result, the ρ_{η_j} obtained in section 4.2 can also be adapted to this case. As we saw previously, if $p = 1$, only the $\rho_{(1,q,0)}$ are not equal to zero and their values have been given in section 4.2. For $p = 3/2$ or $1/2$, we get:

$$\begin{aligned} \rho_{(p,q,0)} \quad & = \sigma \sqrt{X_p^{-3,2}(e_0) K_q^p(\delta, \zeta_0)}, \\ \rho_{(p,q,\pm 1/2)} \quad & = \sigma \sqrt{X_p^{-3,2}(\frac{\Delta e \pm we_0}{2}) K_q^p(\delta, \zeta_0)}, \end{aligned} \tag{54}$$

while the width of the higher order resonant islands is negligible within our approximation. The variations of e and ϖ thus split the eccentric spin

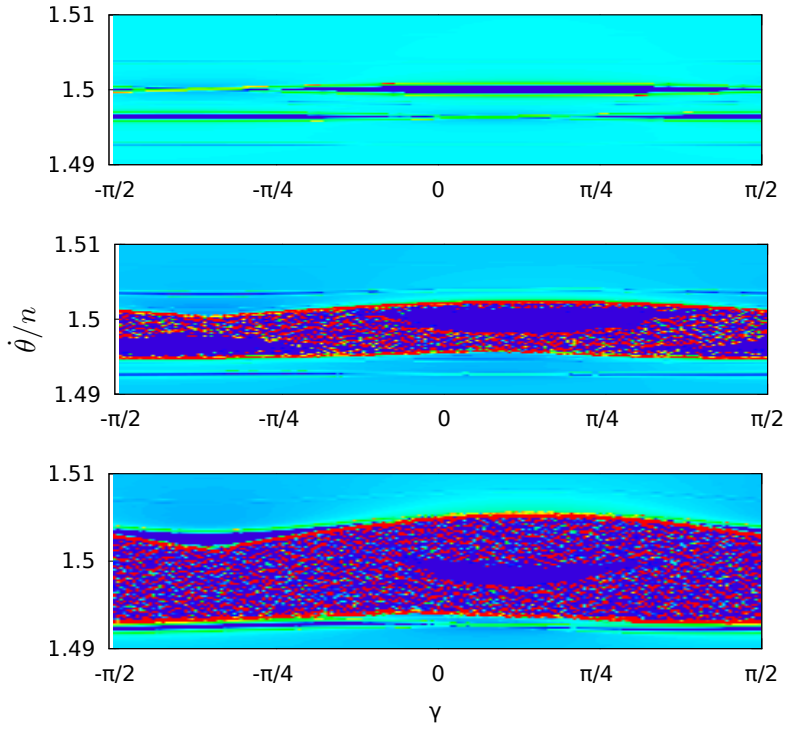

Figure 10: FMA of the phase space $(\dot{\theta}/n, \gamma_p)$ in the neighbourhood of the 3:2 spin orbit resonance, for two coorbitals on tadpole configuration. $e_1 = 0.05$, $e_2 = 0.1$, $m_1 = m_2 = 1 \times 10^{-3} m_0$ and $\zeta_0 = 45°$. We have $\frac{B-A}{C} = 1 \times 10^{-6}$ on the top panel, 1×10^{-5} on the middle one and 5×10^{-5} on the bottom one. See the text for more details.

orbit resonance and the co-orbital spin-orbit resonances into 3 islands, whose center is separated by $g/2$ in the $\dot{\theta}$-direction in the phase space. This new effect on the phase space is more significant for massive co-orbitals. Indeed, we recall that $g = \mathcal{O}(\mu)$, so the more massive the co-orbitals are, the larger the distance between the center of these islands, which increases their impact on the spin dynamics. The islands in $\pm g/2$ are not symmetric, the island in $+g/2$ is always bigger that the one in $-g/2$, which shrinks when $\Delta e \approx e_0 w$. The asymmetry can be seen in the Figure 10: we force e and ϖ to oscillate by adopting different initial eccentricities $e_1 = 0.05$ and $e_2 = 0.1$ for m_1 and m_2, respectively. Focusing on the resonances located at $\eta_j = (3/2, 0, s)$ with $s \in \{-1/2, 0, 1/2\}$ we can see that the islands located at $\pm g/2$ are asymmetric. As shown in equation (54), the island located at $\eta_j = (p, q, -1/2)$ can be of zero-width, while the island located in $\eta_j = (p, q, +1/2)$ can be of commensurate width with $\eta_j = (p, q, 0)$. On the top

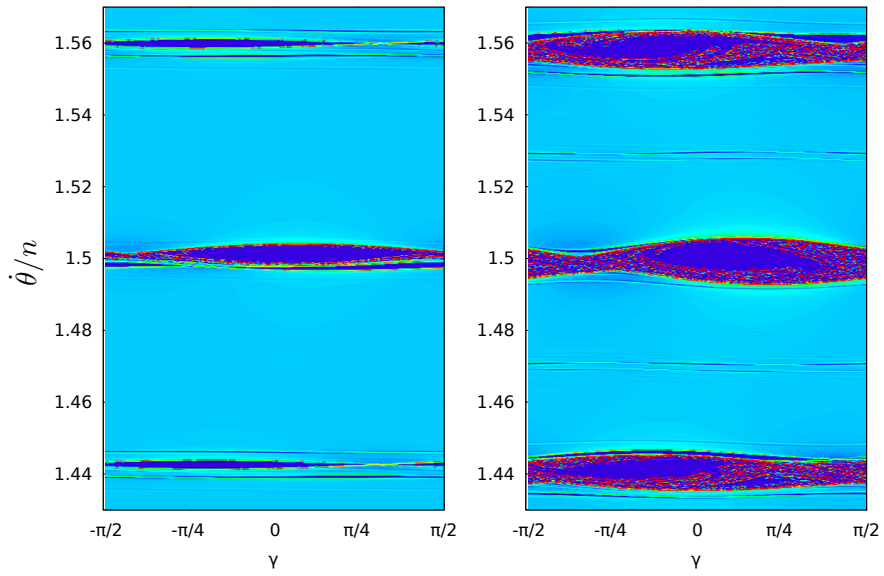

Figure 11: FMA of the phase space $(\dot{\theta}/n, \gamma_p)$ in the neighbourhood of the 3:2 spin orbit resonance, for two coorbitals on tadpole configuration. $e_1 = e_2 = 0.1$, $\frac{B-A}{C} = 5 \times 10^{-5}$ and $\zeta_0 = 45°$ in both cases. On the left $m_1 = m_2 = 1 \times 10^{-3} m_0$ and $m_2 = 2 \times 10^{-3} m_0$, $m_1 = 1 \times 10^{-5}$ on the right. See the text for more details.

panel, the islands at $\pm g/2$ are separated from the main island, while on the two others the three island overlap, ensuring chaos.

In Figure 11 we show another two examples where g is large enough with respect to the island's width, such that it has an impact on the spin dynamics. Here the initial eccentricities have been taken equal, so their oscillation is moderate and the islands in $s = 0$ are sensibly larger than the ones in $s = \pm 1/2$. In both graphs the main 3:2 island is located in $\dot{\theta}/n = 1.5$. The two coorbital spin-orbit resonances located at $\eta_j = (3/2, \pm 1/2, 0)$ are easily identifiable at $\dot{\theta}/n = 1.5 \pm \nu/2 = 1.5 \pm 0.06$. The split of these 3 resonances into 6 additional resonances centred at $\eta_j = (3/2, q, \pm 1/2)$ can be seen on the left panel, where $\delta = 1/2$: $\dot{\theta}/n = 1.5 \pm g/2 = 1.5 \pm 0.0036$ and $\dot{\theta}/n = 1.5 \pm \nu/2 \pm g/2$. On the right panel, the resonance width has been increased by taking a higher value of δ (increasing $(B - A)/C$ would have the same effect). We obtain a phase space that is similar to the one obtained when e and ϖ were considered constant (Fig. 5). However, the overlap with the resonances in $\eta_j = (p, q, \pm 1/2)$ widens considerably the chaotic border of the islands (Morbidelli, 2002, page 222).

6 Conclusion

The presence of a co-orbital companion leads to a perturbation of the true longitude at a frequency of order $\nu = \mathcal{O}(\sqrt{\mu})$. This variation splits the eccentric spin-orbit resonances into new families of co-orbital spin-orbit resonances. Depending on the orbit, on the mass of the two orbiting bodies and on the axial asymmetry of the rotating body, those resonances can give rise to additional resonant islands, a chaotic region, or just widen the separatrix of the already existing islands.

Considering a system of two coorbital planets around a star, one can devise some interesting scenarios: for two super-earth with low asymmetry, their σ is very small compared to ν, thus their resonant islands are relatively thin and spaced from each other. On the contrary, for two earth-like planets, their σ is large enough to a create wide chaotic area. For instance, for two Earth-like co-orbital planets, ν and σ are commensurate ($\sigma/n \approx 7\times10^{-3}$ and $\nu/(2n) \approx 3.5\times10^{-3}$). Finally, if one of the planets is earth-like and the other is a gaseous giant, the phase space of the spin dynamics of the terrestrial planet consists in large separated resonant islands. More generally, due to the diversity of exoplanets and moons, any configuration is possible.

We have shown that co-orbital bodies with low libration amplitude of the resonant angle ζ (tadpole orbits) are likely trapped in a spin-orbit resonance located close to the classic eccentric resonances of the unperturbed problem (Goldreich and Peale, 1966). As the libration amplitude of ζ increases, the co-orbital resonant islands become of commensurable width with the eccentric resonances. In the horseshoe domain, the eccentric spin-orbit resonances are of negligible width with respect to some of the co-orbital resonant island under and above them. In this configuration, the vicinity of the eccentric resonance is generally regular, while it can be surrounded by two chaotic areas created by the overlapping of the main co-orbital resonances.

The co-orbital bodies also mutually perturb the eccentricities and the argument of perihelion of each orbit on a long time-scale of order $\mathcal{O}(\mu)$. The precession of the perihelion has no effect on the phase-space except a slight global offset in the direction of $\dot{\theta}$. However, the frequency g, which rules the libration of the perihelion and the oscillation of the eccentricity, splits both the eccentric spin-orbit families and the co-orbital spin-orbit families into a yet again new resonant family. Nevertheless, in this case the width of the resonant island depends on the variation of the eccentricity and on the argument of perihelion of the rotating body, while its separation to the eccentric or co-orbital spin-orbit resonance is $g/(2n) = \mathcal{O}(\mu)$. Therefore, usually these islands have an insignificant width, or only slightly widen the separatrix of the main resonant islands. However, for systems with low axial asymmetry (low $\frac{B-A}{C}$) and massive co-orbital companions, such as gaseous giants, these resonances can have a significant impact on the spin dynamics.

References

Charlier, C. V. L. (1906). Über den Planeten 1906 TG. Astronomische Nachrichten, 171:213.

Chirikov, B. V. (1979). A universal instability of many-dimensional oscillator systems. Phys. Rep., 52:263–379.

Colombo, G. (1965). Rotational Period of the Planet Mercury. Nature, 208:575.

Correia, A. C. M. (2009). Secular Evolution of a Satellite by Tidal Effect: Application to Triton. apjl, 704:L1–L4.

Correia, A. C. M. and Laskar, J. (2009). Mercury's capture into the 3/2 spin-orbit resonance including the effect of core-mantle friction. Icarus, 201:1–11.

Correia, A. C. M. and Robutel, P. (2013). Spin-Orbit Coupling and Chaotic Rotation for Coorbital Bodies in Quasi-circular Orbits. Astro. physical Journal, 779:20.

Correia, A. C. M. and Rodríguez, A. (2013). On the Equilibrium Figure of Close-in Planets and Satellites. Astro. physical Journal, 767:128.

Danby, J. M. A. (1964). Stability of the triangular points in the elliptic restricted problem of three bodies. Astron. Astrophys., 69:165.

Dermott, S. F. and Murray, C. D. (1981). The dynamics of tadpole and horseshoe orbits. I - Theory. Icarus, 48:1–11.

Gascheau, G. (1843). Examen d'une classe d'quations diffrentielles et application un cas particulier du problme des trois corps. Comptes Rendus, pages 16, 393.

Giuppone, C. A., Beaugé, C., Michtchenko, T. A., and Ferraz-Mello, S. (2010). Dynamics of two planets in co-orbital motion. MNRAS, 407:390–398.

Goldreich, P. and Peale, S. (1966). Spin-orbit coupling in the solar system. aj, 71:425.

Hansen, P. A. (1855). Entwickelung der products einer potenz des radius vectors mit dem sinus oder cosinus eines vielfachen der wahren anomalie in reihen. Abhandl. d. K. S. Ges. d. Wissensch, IV, 182281.

Lagrange (1772). Œuvres complètes VI, 272 . Gouthier-Villars, Paris (1869).

Laskar, J. (1993). Frequency analysis of a dynamical system. Celestial Mechanics and Dynamical Astronomy, 56:191–196.

Leleu, A., Robutel, P., and Correia, A. C. M. (2015). Detectability of quasi-circular co-orbital planets. Application to the radial velocity technique. Astron. Astrophys., 581:A128.

MacDonald, G. J. F. (1964). Tidal Friction. Reviews of Geophysics and Space Physics, 2:467–541.

Mikkola, S., Innanen, K., Wiegert, P., Connors, M., and Brasser, R. (2006). Stability limits for the quasi-satellite orbit. mnras, 369:15–24.

Morais, M. H. M. (1999). A secular theory for Trojan-type motion. Astron. Astrophys., 350:318–326.

Morais, M. H. M. and Namouni, F. (2013). Asteroids in retrograde resonance with Jupiter and Saturn. MNRAS, 436:L30–L34.

Morbidelli, A. (2002). Modern celestial mechanics : aspects of solar system dynamics . (London: Taylor & Francis).

Murray, C. D. and Dermott, S. F. (1999). Solar system dynamics. (Cambridge University Press).

Namouni, F. (1999). Secular Interactions of Coorbiting Objects. Icarus, 137:293–314.

Nauenberg, M. (2002). Stability and Eccentricity for Two Planets in a 1:1 Resonance, and Their Possible Occurrence in Extrasolar Planetary Systems. Astron. J., 124:2332–2338.

Robutel, P. and Laskar, J. (2001). Frequency Map and Global Dynamics in the Solar System I. Short Period Dynamics of Massless Particles. 152:4–28.

Robutel, P., Niederman, L., and Pousse, A. (2015). Rigorous treatment of the averaging process for co-orbital motions in the planetary problem. ArXiv e-prints.

Robutel, P. and Pousse, A. (2013). On the co-orbital motion of two planets in quasi-circular orbits. Celest. Mech. Dyn. Astron., 117:17–40.

Robutel, P., Rambaux, N., and El Moutamid, M. (2012). Influence of the coorbital resonance on the rotation of the trojan satellites of saturn. Celest. Mech. Dyn. Astron., 113(1):1–22.

Wisdom, J., Peale, S. J., and Mignard, F. (1984a). The chaotic rotation of Hyperion. Icarus, 58:137–152.

Wisdom, J., Peale, S. J., and Mignard, F. (1984b). The chaotic rotation of Hyperion. Icarus, 58:137–152.

Wolf, M. (1906). Photographische Aufnahmen von kleinen Planeten. Astronomische Nachrichten, 170:353.

A Appendix

Table 1: Notations. All orbital elements are given in heliocentric coordinates, thus with respect to m_0

variable	definition
a_j	semi-major axis of body j
λ_j	mean longitude of body j
e_j	eccentricity of body j
ϖ_j	argument of periastron of body j
m_j	mass of body j
r_j	distance between m_0 and m_j
f_i	true anomaly of body j
$\bar{a}$	mean semi-major axis of the co-orbital motion
n	mean mean motion, defined from $\bar{a}$
μ	$= (m_1 + m_2)/(m_0 + m_1 + m_2)$
δ	$= m_2/(m_1 + m_2)$
ζ	$= \lambda_1 - \lambda_2$ semi-fast resonant angle
ζ_0	minimum value of ζ on a given orbit
ζ_s	value of ζ at the separatrix between tadpole and horseshoe
ζ_L	value of ζ at the considered Lagrangian equilibrium
z	$= \zeta_0 - \zeta_L$
$\hat{\zeta}$	such that $\hat{\zeta}(\tau) = \zeta(\tau/\nu)$
ν	fundamental frequency for the evolution of ζ
g_1 and g_2	fundamental frequencies for the evolution of (ϖ_1,ϖ_2)
g	$= g_1 - g_2$
$\Delta\varpi$	$= \varpi_1 - \varpi_2$ slow resonant angle
θ	rotation angle of m_1
A, B, C	moment of inertia of m_1
σ	$= n\sqrt{3(B-A)/C}$ asymmetry of the rotating body
ς	$= (n - g_2, \nu, g) \in \mathbb{R}^3_+$ frequency vector
η_j	$= (p, q, s)$ with $2\eta_j \in \mathbb{Z}^3$ identification of a given resonance
ρ_{η_j}	width of the resonance η_j
γ_p	$\theta - pnt$
ϵ_j^k	$= \lvert\langle \eta_j - \eta_k, \varsigma \rangle\rvert$
$X_p^{-3,2}(e)$	Hansen coefficient defined eq. (31)
ξ_l	coefficient of the Fourier expansion of $\hat{\zeta}$
J_k	k^{th} Bessel function

Table 2: $(B-A)/C$ for bodies of the solar system (see Correia and Rodríguez, 2013; Robutel et al., 2012, and references therein). The $(B-A)/C$ of the co-orbitals orbiting around Saturn are so large that their resonant islands totally overlap (Robutel et al., 2012).

body	(B-A)/C	status
Mercury	8.1×10^{-5}	planet
Venus	5.39×10^{-6}	planet
Earth	1.57×10^{-5}	planet
Mars	5.5×10^{-4}	planet
Moon	2.2×10^{-4}	satellite
Io	5.6×10^{-3}	satellite
Europa	1.3×10^{-3}	satellite
Ganymede	3.8×10^{-4}	satellite
Callisto	1.0×10^{-4}	satellite
Rhea	2.4×10^{-3}	satellite
Titan	1.0×10^{-4}	satellite
Polydeuces	2.2×10^{-1}	satellite (tadpole)
Helene	1.3×10^{-1}	satellite (tadpole)
Telesto	3.2×10^{-1}	satellite (tadpole)
Calypso	2.7×10^{-1}	satellite (tadpole)
Janus	1.0×10^{-1}	satellite (horseshoe)
Epimetheus	3.0×10^{-1}	satellite (horseshoe)